

# COMPLETE EULER-SOLUTION FOR A ROTOR IN HOVER AND A PROPELLER IN FORWARD FLIGHT

J. Hertel\*      E. Krämer†      S. Wagner‡

Universität der Bundeswehr München  
Werner-Heisenberg-Weg 39  
8014 Neubiberg, W. Germany

## Abstract

An Euler procedure that is optimized for application on steady rotor flow is presented. For calculation of the flow field of a rotor in hover the initial condition is provided by a prescribed wake model, which allows a significant reduction of the computational domain. The complete rotor or propeller flow field is calculated exclusively by the Euler procedure. Computational results for a model rotor in hover and for a propeller with highly twisted blades in hover as well as in forward flight are presented. The theory is compared with experimental data for the model rotor. Very high angles of attack occur in the root region of the propeller blade. The expected flow separation in this region is reproduced in a qualitatively correct manner.

## Introduction

The efforts to increase the forward speed of a helicopter and/or to reduce the noise emission caused by the rotor can be met with success only by detailed investigation of the flow field in the blade vicinity. The transonic flow occurring at the blade tip requires the application of nonlinear methods such as potential (Ref 1-5), Euler- (Ref 6-10) or Navier-Stokes procedures (Ref 11-13). These approaches are well proved for fixed wing calculations and nowadays also for rotor flow field computations. Which kind of analysis is used depends on computational resources, accuracy requirements and available manpower. However, modern supercomputers allow a wide application of Euler- and even Navier-Stokes methods also in rotorcraft aerodynamics (Ref. 14). Nevertheless, an appropriate modelling of the aerodynamic problem still remains to be the key task of the engineer. This concerns, there are the generation of a suited grid, the formulation of the boundary condition and the modelling of the blade-vortex-interaction, which has a considerable influence on the blade aerodynamic,

especially in the hover flight.

The blade-vortex-interaction can either be approximated by a wake model, necessary for potential methods, or can be captured by the Euler- or Navier-Stokes procedure itself. The majority of the methods mentioned above uses a prescribed or a free wake model and depends herewith on the accuracy of such a modelling. In order to avoid this disadvantage, an Euler procedure is developed that starts with an initial condition provided by a prescribed wake model. Afterwards, the Euler procedure drives the iteration to a convergent solution only by itself, without any using of external aids. This approach is presented in this paper, which is a continuation of the work presented on the AIAA 8th Applied Aerodynamics Conference (Ref 15).

The present Euler procedure has been derived from the EUFLEX-Code developed by Eberle (Ref 16). The code is well proved for fixed-wing applications. It is an upwind finite-volume Godunov-scheme and solves a 1-D Riemann problem. The code is third order accurate and is switched to first order at shocks. The prescribed wake model providing, the initial condition for the Euler procedure, is composed of the model of Landgrebe (Ref 17) to determine the geometry of the inboard helical vortex sheet, and of the model of Kocurek (Ref 18, 19) to determine the tip vortex path. The helical vortex sheet and the tip vortex are enclosed by a bounded vortex at the blade and by the "classical" starting vortex at the end of the sheet (Fig 1). In this way the vorticity conservation of the wake construction is ensured. The complete rotor wake represents a steady state solution, so that the time consuming calculation of the starting process, as reported in Ref 15, can be omitted.

The wake solution is transferred in terms of flow variables into the cell mid points by Biot-Savart's Law (velocity components) and by the isentropic relation (density and pressure). This solution provides the initial condition and the far-field boundary condition for the Euler calculation. By application of such a consistent far-field boundary condition the computational domain can be reduced remarkably,

\*MTU Munich

†MBB Munich

‡Professor, Aerospace Engineering

which leads to an overall computational time saving of more than 50%. In order to validate the code, computations were performed for the model rotor of Caradonna & Tung (Ref 20). The comparison of computed results with experimental data shows a very good agreement for moderate angles of attack.

Beside this, calculations were performed for a highly twisted propeller-like rotor in hover and axial flight. Due to very high angles of attack in the root region of the blade in case of hover flight, the expected flow separation on the upper side was reproduced in a realistic manner. The separation region is enclosed by two vortices, which completely change the figure of the classical wake. The results are presented and discussed. The calculation of the configuration in a fast axial flight shows a very weak blade-vortex-interaction that can be treated by a usual CFD approach and a relatively small computational domain.

### Numerical Method

The Euler procedure used is based on governing equations formulated within a blade-attached cylindrical coordinate system in accordance with the flow field of a rotor. The reference frame rotates with the angular velocity  $\vec{\omega}$  of the rotor. In order to avoid the dependence of the flux calculation upon the circumferential term  $\vec{\omega} \times \vec{r}$ , the approach uses absolute flow values. Thus, the centrifugal and Coriolis' forces are only considered as far as they are caused by induced velocities.

The numerical algorithm of the procedure was originated by Eberle (Ref 16) and adjusted for computation of flow fields for rotors in hover or axial forward flight by the authors (Ref 9, 21, 22, 23). It is a Godunov-type algorithm, which solves the 1-D Riemann problem by an upwind scheme in each spatial direction in a grid conform coordinate system. The code is third order accurate in space, and is switched to first order at shocks. Thus, it provides a relatively low numerical dissipation. This is essential for a correct transportation of vorticity over a long distance within the computational domain as e.g. in a flow field of a rotor in hover. The vorticity conservation of the code was successfully proved (Ref 21). Since only steady cases were computed, local time stepping was used, and the code could be run with first order time accuracy. The presented results were performed by a time explicit scheme. However, a time implicit code based on the pointwise Gauss-Seidel relaxation method is also in use (Ref 23). A more detailed description of the method can also be found in Ref 15.

### Computational Grids

The demand to compute the complete rotor flow field exclusively by the Euler procedure leads to a computational domain that encloses the rotor disk. For steady state calculations this requirement can

be met by applying the periodic condition to a grid, which encloses only one blade. Additionally, the grid remains time invariant during the Euler calculation.

### Grid Generation

The results presented herein were obtained with an H-H-type grid. A grid of that kind is shown in Fig 2. It was generated for the two-bladed model rotor measured by Caradonna & Tung (Ref 20). Since the periodic condition in circumferential direction is applied at the inflow and outflow planes, the grid encloses only one half of the rotor flow field. The point distribution in the outflow plane matches the points in the inflow plane. Thus, the formulation of the periodic condition is very simple and does not require any interpolations of the flow values between the corresponding cells. The H-topology provides a fine and equal space discretization even in the farfield of the computational domain. This is essential for vortex transport. On the other hand, this feature leads to a deficiency of the H-topology, since a very high number of grid points is placed in regions, where it is not necessary. Thus, above the blade and in the outer coaxial cylindrical grid planes, where no vortex flow occurs, the resolution has not to be so fine.

The grid generation is performed by an elliptic differential procedure. The grid points are found by solving a system of Poisson's and Laplace's differential equations. This approach provides a very homogenous point distribution, which is advantageous for an accurate vorticity transport in conjunction with fine resolution. The procedure is described in detail in Ref 23.

### Geometry of the Configurations

Model Rotor To verify the Euler results, which were obtained by a calculation starting from the initial condition that is provided by the prescribed wake model, a computation of a test case for the model rotor was performed. Fig 2 shows the computational grid for this calculation. The complete rotor blade up to the axis of rotation is enclosed by the grid. For the test case presented the blade is embedded with a pitch angle of 5°, so that the grid cylinder axis is colinear with axis of rotation. The blade of this configuration has a rectangular shape and a radius of 6 chord lengths. The physical extension of the grid is 4 chord lengths above and 6 below the rotor disk as well as 12 chords in radial direction. The total number of grid points is 87 × 33 × 33 in circumferential, radial and axial direction respectively. However, for this configuration such a physical extension of the computational domain would be too small if a conventional procedure was applied, as shown in Ref 15. Nevertheless, it is large enough for a computation starting from an initial and far-field boundary condition, provided by the wake model.

Propeller Configurations Additionally, computations for a rotor with highly twisted blades and for

a propeller with the same blade geometry were performed, in order to investigate the behaviour of the Euler solutions in cases of extreme flow conditions.

The computed configuration is a rotor with three rectangular blades with a spanwise twist angle of  $-44^\circ$ . The blade is fixed to a spinner, whereby it is tapered at the root to half a chord length. The blade surface grid is shown in Fig 3.a. In the inner region a very thick airfoil (28% thickness) was used, which was originally developed for rotors of wind energy converters. The thickness of the used airfoils reduces smoothly up to 9% at the tip. The blade has a radius at the one quarter point of 8 chord lengths of the rectangular part of the blade.

The complete grid for this configuration is displayed in Fig 3.b. Since a three-bladed rotor is considered, the angle of aperture of the grid is  $120^\circ$ . The spinner is also enclosed in the grid and is approximated by an ellipsoid lengthed by a cylinder. The blade is embedded in the grid with a collective pitch angle that leads to a local angle of incidence of approximately  $40^\circ$  in the inner region. Similar to the model rotor grid, the physical extension of the computational domain for this configuration is 0.65 and 1.15 times the rotor radius above and below the rotor disk respectively as well as twice the rotor radius to outer surface of the grid. The total number of grid points is  $77 \times 45 \times 45$  nodes.

Since the collective pitch angle of the blade is the only difference between the configurations for the hover and for the axial forward flight, the grid for the forward flight computation will be shown in the results. Besides, the topology of the blade embedding had to be changed due to very high angles of incidence related to the circumferential direction. Thus, the blade is embedded between two vertical planes of the grid for calculating the forward flight in contrast to the embedding between two horizontal planes for hover computations. The total amount of grid points remains the same, however, the number in circumferential and the number in axial direction was interchanged:  $45 \times 45 \times 77$  nodes.

### Initial and Boundary Conditions

Beside the numerical algorithm and the computational grid, the boundary conditions are very significant topics of the complete CFD procedure. Since the final result of the calculation depends on the far field boundary condition, it has to be formulated very carefully. On the other hand, the initial condition influences a numerical steady state solution only in cases of extreme flow conditions.

### Boundary Conditions

In this code the nonreflecting characteristic far-field boundary condition was used at the top and at the outer circumferential boundary. At the bottom

of the computational domain the nonreflecting condition was modified for hover calculations: All flow values, except the vertical component of the velocity, are calculated at the bottom grid plane by an arithmetic averaging of the undisturbed flow values and of the values extrapolated from the interior of the computational domain. For the calculation of density and pressure the isentropic relation was used as it is formulated in Ref 24. The vertical velocity component is computed by a weighted extrapolation from the interior and an averaging with the undisturbed value:

$$w_1 = \frac{(1.25w_2 - 0.25w_3) + w_\infty}{2}$$

With indices indicating the cell numbers in  $z$ -direction,  $w$  means the  $z$ -component of the velocity vector. For the computation of the axial forward flight the same nonreflecting condition as at the top of the computational domain was used at the bottom, since the induced downwash velocity in this plane is much smaller than the axial flight velocity.

At the blade and at the spinner the tangency condition was used, ensuring that the fluxes through the blade surface are equal to zero. Besides, at the inflow and outflow planes in circumferential direction the periodic condition was applied in order to compute the blade-vortex-interaction.

### Initial Condition

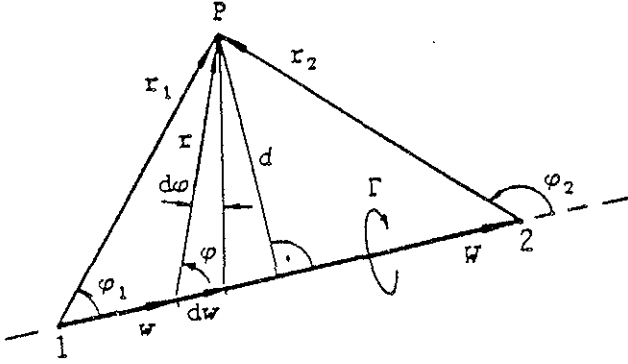
Usually a free stream condition is used as an initial state of the flow field. During the computation the flow field is changed continuously until the steady state is reached. This process is comparable with a starting process in the nature. For the calculation of the axial forward flight this condition is sufficient, since the starting vortices leave very fast with (approximately with the free stream velocity) the computational domain. On the other hand, in the flow field of a rotor in hover the downwash is induced by a vortex cylinder consisting of tip vortices. Since the development of the cylinder depends on the induced velocities of the wake, this process is lasting a very long period of time (Ref 15). CFD procedures like Euler or Navier-Stokes codes, which allow to compute anisentropic flow, are able to reproduce this phenomenon, but spends a lot of computational time. Additionally, it requires a large computational domain that allows the starting vortex to descent far enough from the rotor disk.

In order to reduce the computational domain the initial condition was approximated by a steady state solution resulting from a prescribed wake model. Additionally, the far-field boundary conditions were also obtained from the prescribed wake solution. The prescribed wake model provides the geometry of the helical wake and of the path of the tip vortex (Fig 1), with the vortex filaments being approximated by short straight vortex lines with the circulation  $\Gamma$ . By

applying Biot-Savart's Law the induced velocity vector  $\vec{V}_P$  can be calculated as follows:

$$\vec{V}_P = \frac{\Gamma}{4\pi} [1 - e^{-(d/r_D)^2}] \cdot \frac{\vec{r}_1 \times \vec{W}}{d \cdot |\vec{r}_1 \times \vec{W}|} (\cos \varphi_1 - \cos \varphi_2)$$

with  $r_D$  being the damping radius of a Oseen's viscous vortex. The notation used for geometrical values is explained in the sketch below:



Density and pressure can be derived from the isentropic relation and from Bernoulli's equation:

$$s - s_\infty = c_p \cdot \ln \left[ \frac{\rho_\infty}{\rho} \left( \frac{p}{p_\infty} \right)^{\frac{1}{\kappa}} \right] = 0$$

and

$$a^2 = a_\infty^2 - \frac{\kappa - 1}{2} \bar{q}^2$$

which leads to

$$\rho = \rho_\infty \left( \frac{a}{a_\infty} \right)^{\frac{2}{\kappa - 1}}$$

$$p = p_\infty \left( \frac{a}{a_\infty} \right)^{\frac{2\kappa}{\kappa - 1}}$$

with  $a$  being the sound velocity,  $\rho$  the density,  $p$  the pressure and  $\bar{q}^2 = |\vec{V}_p|^2$  the square of the induced velocity. Thus, all flow values for inviscid flow can be calculated.

## Computational Results

### Model Rotor

The calculation for the model rotor was performed for a tip Mach number of 0.815 and a collective pitch angle of  $5^\circ$  in order to validate the modified initial and far-field boundary condition provided by the prescribed wake model. The flow field evolution beginning with the initial condition is shown in Fig 4. The very large velocity vectors in the wake solution are caused by a small vortex core (damping) radius chosen for the determination of the induced velocities by Biot-Savart's Law. Nevertheless, the flow field is smoothed by the Euler calculation very rapidly (Fig 5.b,c). It is remarkable that the Euler results shows the expected tip vortex contraction. The computation was performed on CONVEX C202 mini-super

computer, so the computer time consumption is given for this computer performance (Fig 4 and 5).

The computational results are validated by comparison with experimental data. Fig 5 displays the measured and calculated pressure distribution for different radial stations. The agreement is very good, especially at the outermost radial station  $r/R = 0.96$ . This fact proves that the blade-vortex-interaction is reproduced correctly.

The time evolution and the final lift distribution are displayed in Fig 6. The deviations between analysis and experimental data are obviously due to viscosity and measurement faults. A more detailed temporal evolution of the lift at a radial station  $r/R = 0.97$  is shown in Fig 7. The integral value shows a very sensitive variation that depends on the temporal wake changes caused by the Euler calculation.

This calculation has shown that the prescribed wake model provides a very coarse approximation of the Euler solution. Since the circulation of the vortex and of the wake changes during the Euler calculation, the iteration itself needs approximately the same time as a calculation starting from free stream initial condition. Nevertheless, the application of the wake model solution as initial and far-field boundary condition allows a significant reduction of the size of the computational domain and herewith of the computational expense.

### Propeller in Hover

The second configuration presented is a propeller-like rotor with highly twisted blades. The computation for this configuration was performed only with the free stream initial condition. Nevertheless, the result shows a nearly steady state solution in blade vicinity. The tip Mach number for this calculation was  $M_{tip} = 0.629$  and the collective pitch angle was  $47^\circ$  corresponding to an angle of incidence of  $3^\circ$  at the blade tip. The periodic condition was applied at the outflow and the inflow grid planes in circumferential direction was applied. Thus, the blade-vortex-interaction was computed by the Euler procedure only.

Due to very high angles of attack up to  $44^\circ$  in the inner region of the blade, a flow separation region was expected. This phenomenon was reproduced by the Euler procedure and is displayed in Fig 8. The "Euler-separation" occurs as a counterrotating vortex, which extends up to 70% of the blade span. The next figure shows the pressure distribution related to sound dynamic pressure at different radial stations (Fig 9). The picture displays a very low pressure level in the separation region. However, the counterrotating vortex is an inviscid approximation of a viscous phenomenon and does not represent the real structure of a flow separation.

The local Mach number distribution in the grid plane containing the upper side of the blade clearly displays the extension of the separation (Fig 10). Since the Euler procedure provides the conservation of vorticity, the counterrotating vortex due to the separation has to be enclosed by a third vortex, which has the same direction as the two classical tip vortices and deforms the blade wake. The origin of this vortex is visible at the end of the separation region. This is confirmed by the next picture (Fig 11) showing the circulation distribution  $\frac{d\Gamma}{ds}$  in a Trefftz plane at  $\varphi = 45^\circ$ . Shadows of the tip vortex and of the separation vortex are displayed very clearly.

The results of the computation show the capability of the Euler procedure to reproduce and to overcome separated flow. However, the result cannot be evaluated quantitatively, and it indicates that the separation leads to an unexpected "unclassical" helical wake structure.

### Propeller in Forward Flight

The propeller blade was installed with a collective pitch angle of  $87^\circ$  for forward flight conditions. The calculation was performed for a circumferential Mach number of  $M_{cir} = 0.568$  and an axial or flight Mach number of  $M_\infty = 0.498$ . In conjunction with the geometry of the blade this flight condition leads to an effective angle of attack of  $2^\circ$ , which is nearly constant along the blade span. The computational grid for this configuration is shown in Fig 12. In this case the blade is embedded between two vortical grid planes. The blade rotates in counterclockwise direction, thus the axial flow moves in negative  $z$ -direction.

The computational result shown in Fig 13 in terms of local Mach number distribution on the blade surface shows two critical regions on the upper side — at the blade root due to the very high thickness (28%) and at the blade tip due to the high Mach number ( $M_{tip} = 0.755$ ). The pressure distribution displayed in Fig 14 indicates a very high pressure gradient in the rear part in the root section ( $r/R = 0.3$ ), which obviously leads to flow separation in a real viscous flow. However, the thickness and twist distribution chosen for this configuration led to a smooth load distribution on the blade in forward flight.

In contrast to the significant influence of the blade-vortex-interaction on the blade load in hover, the interaction between the blade and the tip vortices in forward flight condition is much smaller. Fig 15 shows the circulation distribution in a grid plane parallel to the rotor disk at  $z/C = 4.5$ , with  $C$  representing the chord length. The picture displays the shadows of the inboard and of the tip vortices. One can recognize a very fast movement of the vortices away from the blade and out of the computational domain. Thus, the blade-vortex-interaction is nearly as easy to treat in a high speed forward flight as in fixed wing

computations.

### Conclusions

The modification of the initial and the far field boundary conditions provided by a prescribed wake model for an Euler procedure was presented. It was found that it is a promising way to save computational time by reducing the size of the physical domain. However, the blade-vortex-interaction was calculated by the Euler procedure itself in a closed computational domain. The validation of the procedure was performed by computation of a transonic test case for the model rotor. The results are in very good agreement with the experimental data.

The calculation of a rotor with highly twisted blades showed the robustness of the code even in regions where the flow is separated. The flow separation is reproduced as a vortex, which is an inviscid approximation of the viscous phenomenon. Therefore, the quantitative results in this region are rather poor.

Additionally, calculation for a propeller with the same blade geometry was performed for the axial forward flight condition. The result showed the necessity to design the blade airfoil and shape very carefully at the tip as well as at the root.

### Acknowledgements

The computations of the propeller in hover and in forward flight were performed in cooperation with MBB, Helicopter Division. The authors would like to acknowledge the support by the MBB company.

### References

1. Caradonna, F.X., Tung, C. and Desopper, A., "Finite-Difference Modelling of Rotor Flows Including Wake Effects", AHS-Journal, Vol. 29, Apr. 1984, pp. 26-33.
2. Chang, I-C. and Tung, C., "Numerical Solution of the Full-Potential Equation for Rotors and Oblique Wings Using a New Wake Model", AIAA-Paper 85-0268, 1985.
3. Egolf, A. and Sparks, P., "Hover Rotor Airload Prediction Using a Full Potential Flow Analysis with a Realistic Wake Geometry", 41st Annual Meeting of the AHS, Ft. Worth, TX, 1985.
4. Strawn, R.C. and Caradonna, F.X., "Numerical Modelling of Rotor Flows with a Conservative Form of the Full-Potential Equations", AIAA-Paper 86-0079, 1986.
5. Steinhoff, J. and Ramachandran, K., "A Vortex Imbedding Method for Free Wake Analysis of Helicopter Rotor Blades in Hover", 13th European Rotorcraft Forum, Arles, France, Sep. 1987, Paper-No. 2-11.

6. Wake, B.E., Sankar, N.L. and Lekoudis, S.G., "Computation of Rotor Blade Flows Using the Euler Equations", *Journal of Aircraft*, Vol. 23, 1986, pp. 582-588.
7. Agarwal, R.K. and Deese, J.E., "Euler Calculation for Flowfield of a Helicopter Rotor in Hover", AIAA-Paper 86-1782, 1986.
8. Kroll, N., "Computation of the Flow Fields of Propellers and Hovering Rotors Using the Euler Equations", 12th European Rotorcraft Forum, Garmisch-Partenkirchen, Germany, Sep. 1986, Paper-No. 28.
9. Krämer, E., Hertel, J. and Wagner, S., "The Study of the Wake Influence of a Helicopter Rotor Blade on the Following Blades Using Euler Equations", 14th European Rotorcraft Forum, Milano, Italy, Sep. 1988, Paper-No. 6.
10. Cheng, C.L. and McCroskey, W.J., "Numerical Simulation of Helicopter Multi-Bladed Rotor Flow", AIAA 26th Aerospace Science Meeting, Reno, NV, Jan. 1988, Paper-No. 88-0046
11. Wake, B.E. and Sankar, N.L., "Solution of the Navier-Stokes Equations for the Flow About a Rotor Blade", National Specialists Meeting on Aerodynamics and Aeroacoustics, Arlington, TX, Feb. 1987.
12. Agarwal, R.K. and Deese, J.E., "Navier-Stokes Calculation of the Flowfield of a Helicopter Rotor in Hover", AIAA 26th Aerospace Science Meeting, Reno, NV, Jan. 1988, Paper-No. 88-0046
13. Srinivasan, G.R. and McCroskey, W.J., "Navier-Stokes Simulation of Unsteady Three-Dimensional Blade-Vortex Interactions", 45th Annual Forum of the AHS, Boston, MA, May 1989.
14. McCroskey, W.J., "Some Rotorcraft Applications of Computational Fluid Dynamics", 2nd International Conference on Rotorcraft Basic Research, College Park, MD, Feb. 1988.
15. Krämer, E., Hertel, J. and Wagner, S., "Euler Procedure for Calculation of the Steady Rotor Flow with Emphasis on Wake Evolution", AIAA, 8th Applied Aerodynamics Conference, Portland, OR, Aug. 1990.
16. Eberle, A., "A New Flux Extrapolation Scheme Solving the Euler Equations for Arbitrary 3-D Geometry and Speed. MBB-EUFLEX", MBB/LKE/122/S/PUB/140, 1984.
17. Landgrebe, A., "An Analytical and Experimental Investigation of Helicopter Rotor Hover Performance and Wake Geometry Characteristics", United Aircraft Corporation Research Laboratories, East Hartford, CT, USAAMRDL TR 71-24, June 1971.
18. Kocurek, J.D., Berkowitz, L.F. and Harris, F.D., "Hover Performance Methodology at Bell Helicopter Textron", 36th AHS Annual Forum, Washington D.C., May 1980, Paper-No. 80-3.
19. Kocurek, J.D., "A Lifting Surface Performance Analysis with Circulation Coupled Wake for Advanced Configuration Hovering Rotors", Ph.D. Dissertation, Texas A&M University, May 1979.
20. Caradonna, F.X. and Tung, C., "Experimental and Analytical Studies of a Model Helicopter Rotor in Hover", NASA TM-81232, 1981.
21. Hertel, J., Krämer, E. and Wagner, S., "Euler Solutions for Steady Flow of a Helicopter Rotor", Second International Conference on Rotorcraft Basic Research, College Park, MD, Feb. 1988.
22. Hertel, J., "Euler-Lösungen der stationären Rotorströmung für den Schweb- und den axialen Vorwärtsflug mit Einbeziehung linearer Methoden", Dissertation, Universität der Bundeswehr München, in preparation.
23. Krämer, E., "Theoretische Untersuchungen der stationären Rotorblattumströmung mit Hilfe eines Euler-Verfahrens", Dissertation, Universität der Bundeswehr München, in preparation.
24. Chang, I-C. and Tung, C., "Euler Solution of the Transonic Flow for a Helicopter Rotor", AIAA-Paper 87-0523, 1987.

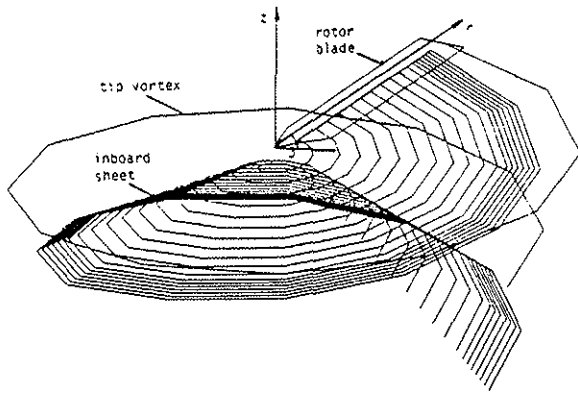


Figure 1: Prescribed wake model and blade attached cylindrical coordinate system.

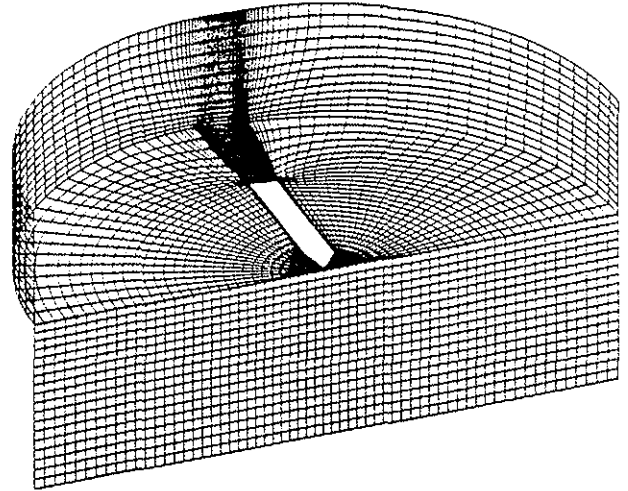
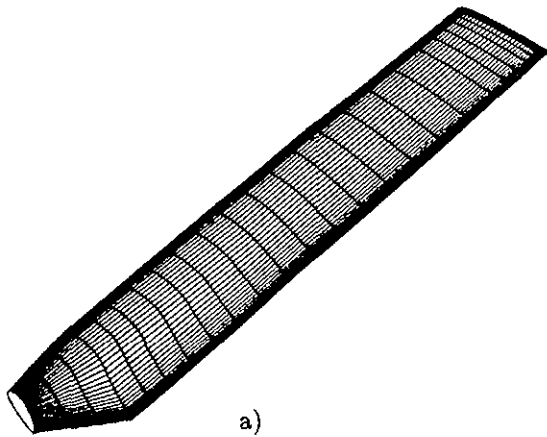
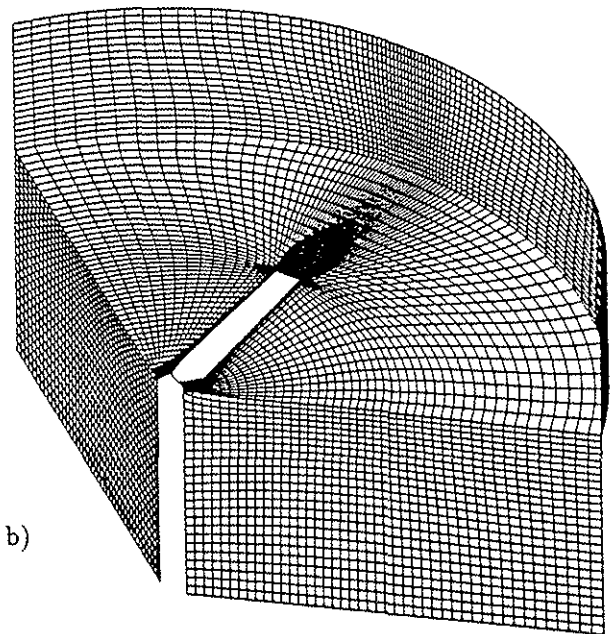


Figure 2: H-H-type grid for the model rotor calculation (Ref 20).

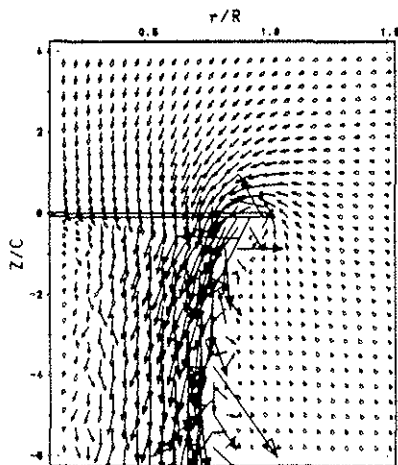


a)

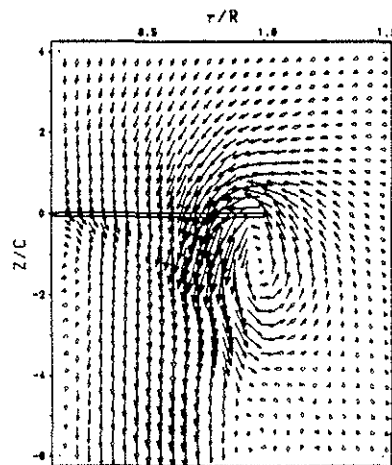


b)

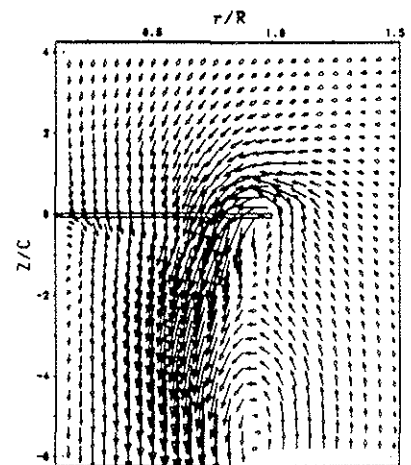
Figure 3: Blade surface grid and isometric view of the complete computational grid for propeller in hover calculation.



a) Initial condition



b) after  $2.2 \cdot 10^5$  CPU-sec.



c) after  $5.2 \cdot 10^5$  CPU-sec.

Figure 4: Flow evolution during the Euler calculation in a Trefftz' plane at  $\varphi = 60^\circ$ .

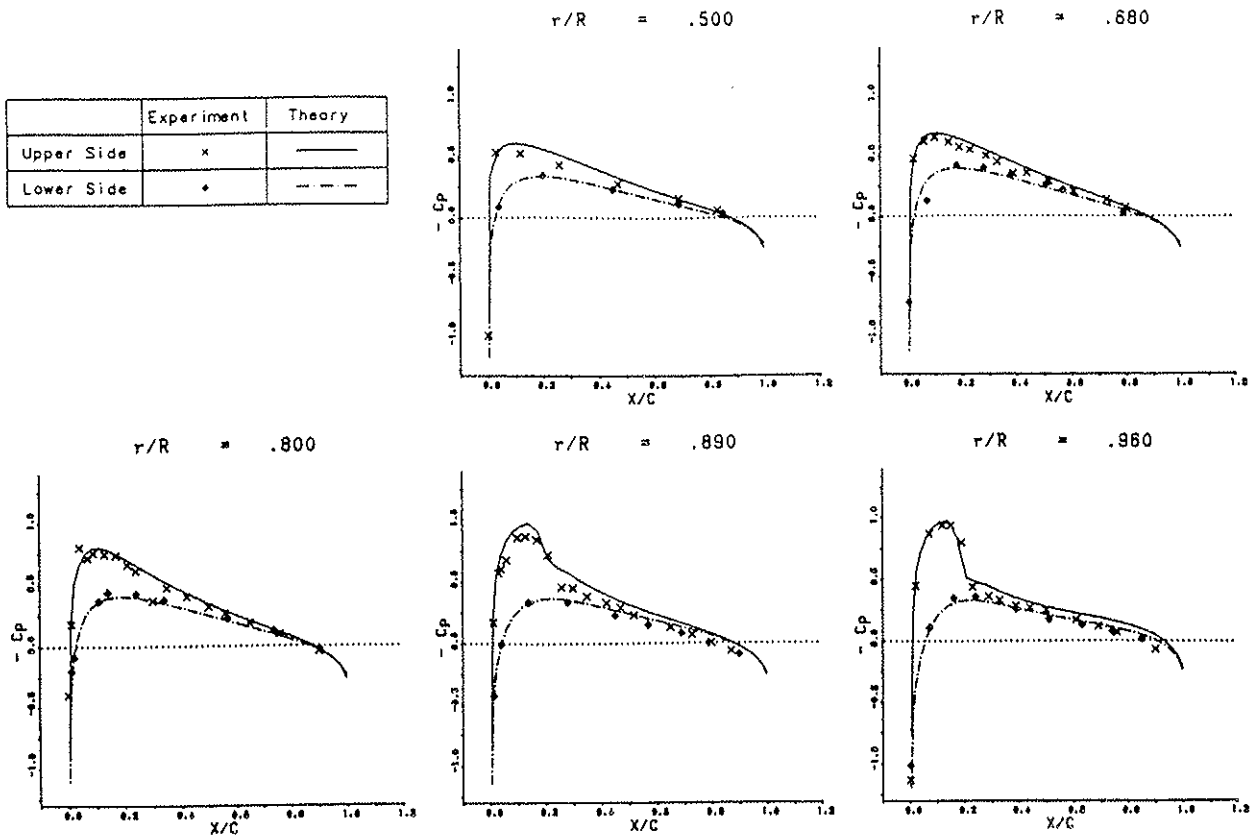


Figure 5: Pressure distribution for the model rotor at  $M_{tip} = 0.815$  and a collective pitch angle of  $5^\circ$  after  $5.2 \cdot 10^5$  CPU-sec. Experimental data from Ref 20.

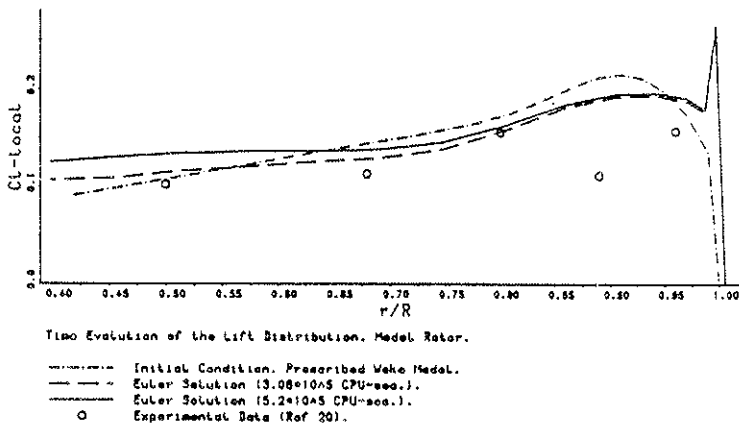


Figure 6: Temporal evolution of the lift distribution for the model rotor.

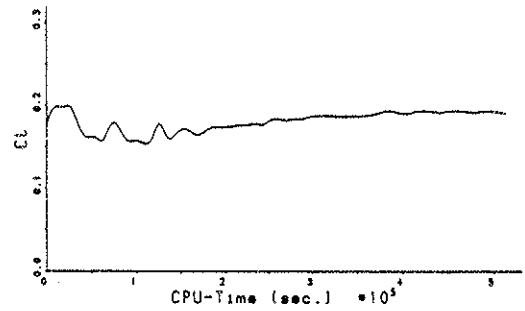


Figure 7: Lift evolution for the model rotor at the radial station  $\frac{r}{R} = 0.97$ .

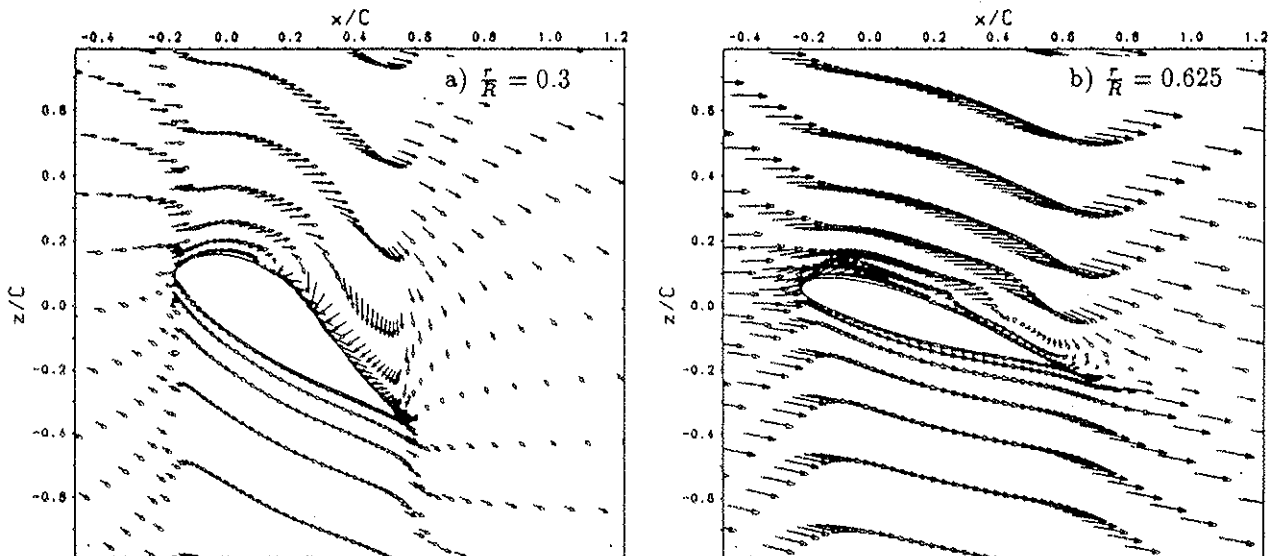


Figure 8: Flow field in two cross sections for propeller in hover.

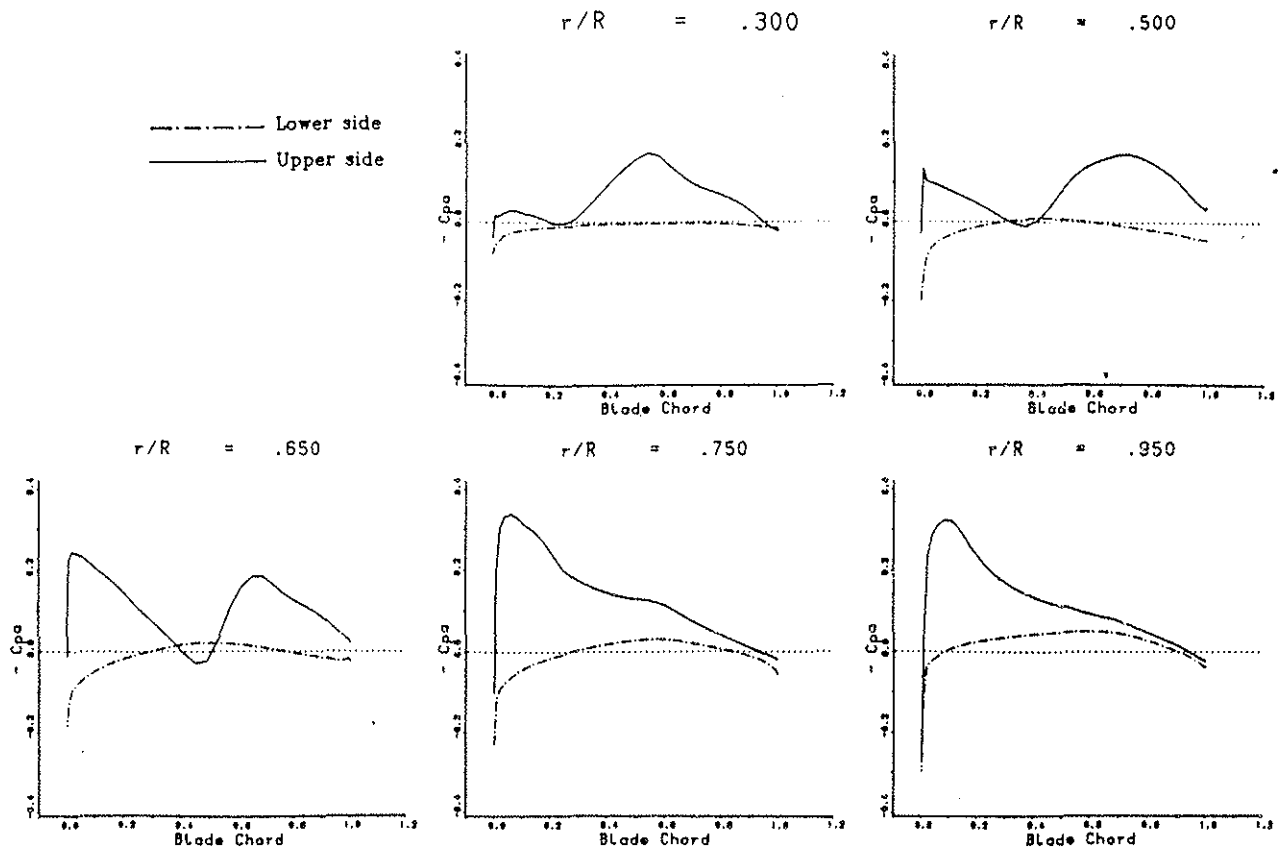


Figure 9: Pressure distribution for propeller-like rotor in hover at  $M_{tip} = 0.629$  and a collective pitch angle of  $47^\circ$ .

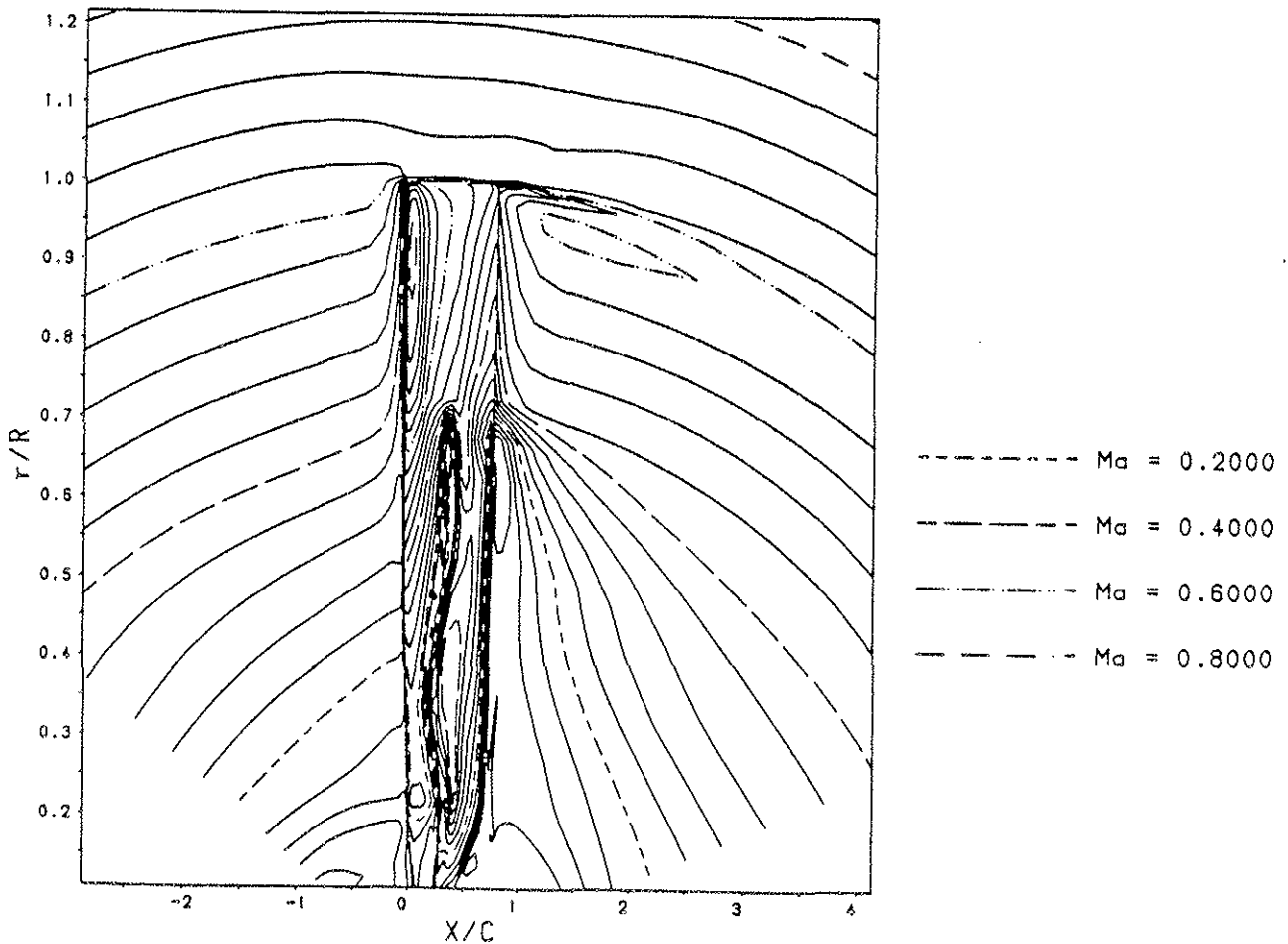


Figure 10: Local Mach number distribution in the plane through the upper side of the propeller-like rotor in hover.

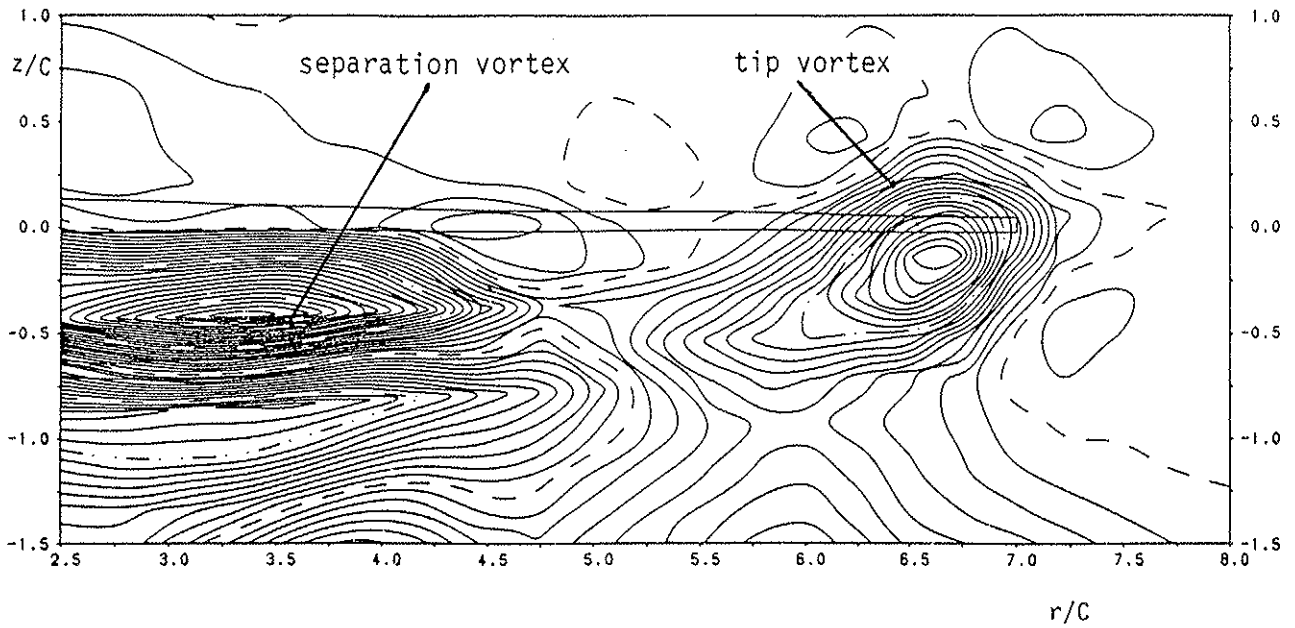


Figure 11: Circulation density distribution  $\frac{d\Gamma}{ds}$  for propeller in hover in a Trefftz' plane  $\varphi = 45^\circ$ .

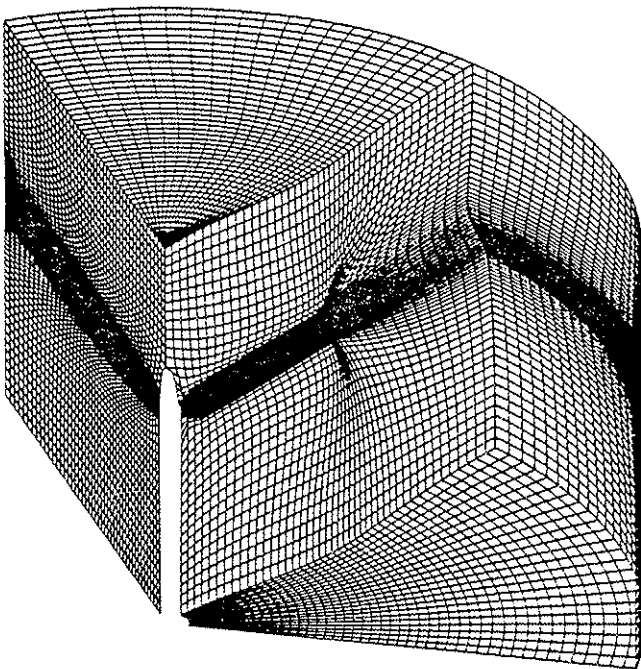


Figure 12: Isometric view of the H-H-type grid for a propeller in forward flight computation ( $45 \times 45 \times 77$  grid points).

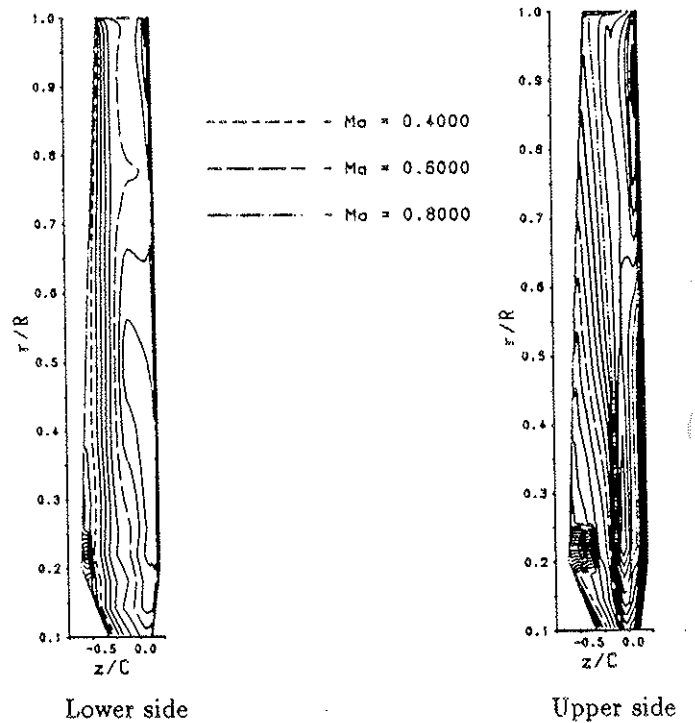


Figure 13: Local Mach number distribution on the blade surface for a propeller in forward flight for a circumferential tip Mach number  $M_{cir} = 0.568$ ,  $M_\infty = 0.498$  and a collective pitch angle of  $87^\circ$ .

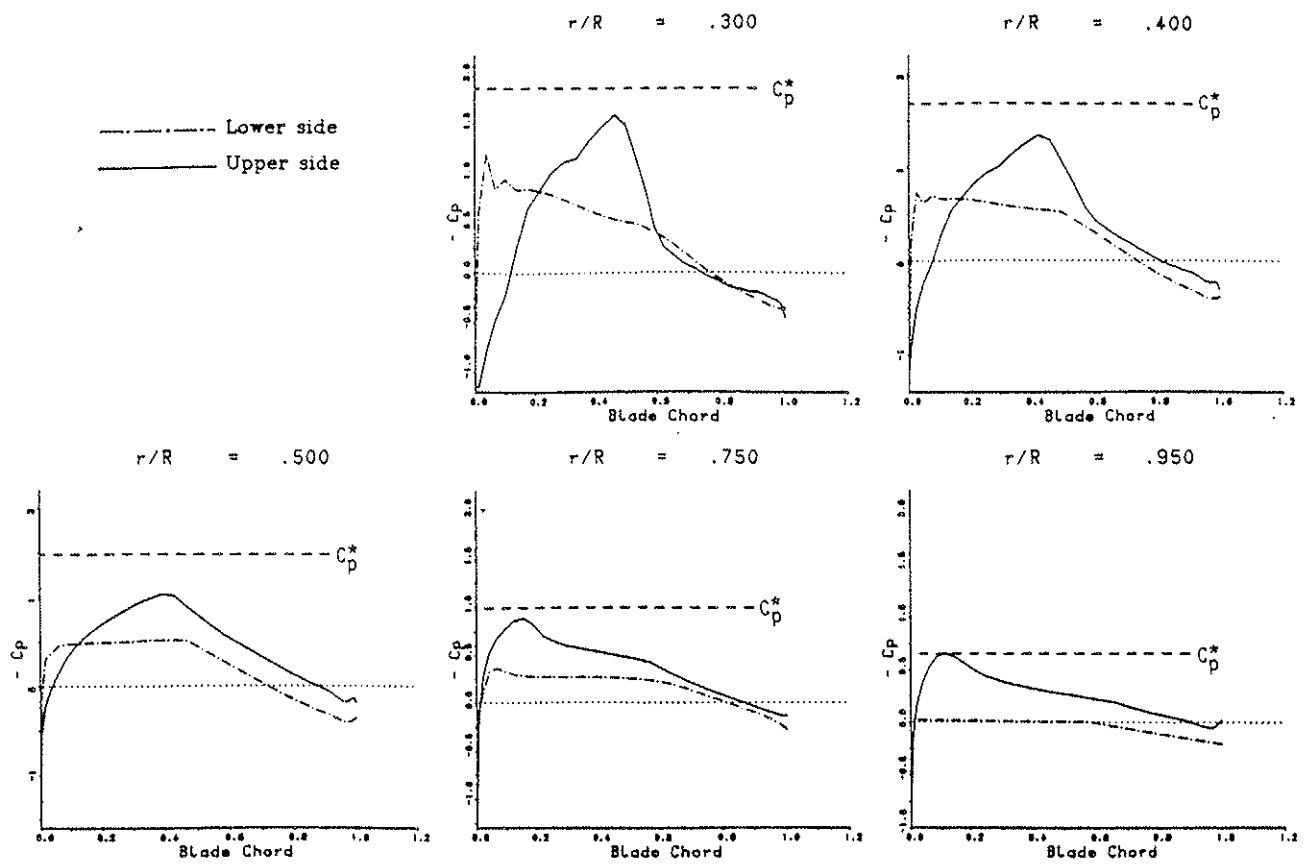
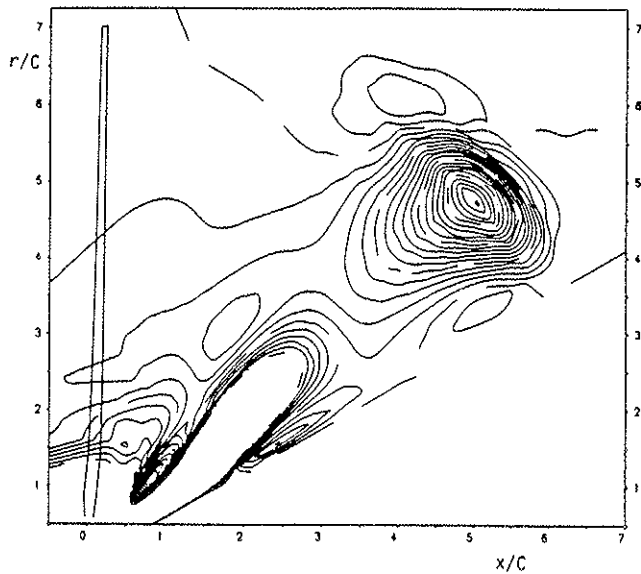


Figure 14: Pressure distribution for a propeller in forward flight for a circumferential tip Mach number  $M_{cir} = 0.568$ ,  $M_{\infty} = 0.498$  and a collective pitch angle of  $87^\circ$ .



Plane  $z/C = -4.5$

Figure 15: Circulation density distribution  $\frac{d\Gamma}{dS}$  for a propeller in forward flight in a plane normal to the  $z$ -direction at  $\frac{z}{C} = -4.5$ .